

Kosterlitz-Thouless phase and continuous melting transition in layered superconductors immersed in a parallel magnetic field

Xiao Hu and Masashi Tachiki

Computational Materials Science Center

National Institute for Materials Science, Tsukuba 305-0047, Japan

(revised on April 24, 2003)

Abstract

$B - T$ phase diagram with a multicritical point for interlayer Josephson vortices is mapped out based on Monte Carlo simulations. For high magnetic fields we find a novel Kosterlitz-Thouless (KT) intermediate phase characterized by in-plane two-dimensional (2D), quasi long-range orders (QLROs) of vortex alignment and superconductivity. Both the transition to high-temperature normal state and the evolution to low-temperature phase of 3D LRO are continuous. Decoupling of the 3D system into the 2D state is triggered by hops of segments of Josephson flux lines across superconducting layers activated by thermal fluctuations. For low magnetic fields, a single first-order melting transition is observed.

PACS numbers: 74.60.Ge, 74.20.De, 74.25Bt, 74.25.Dw

The discovery of high- T_c superconductivity in cuprates has triggered extensive researches into the finite-magnetic-field superconductivity transition in type II superconductors [1]. It is now well established that the transition is first order, accompanied by the freezing of the flux-line liquid into lattice. This notion is particularly important because the transition was considered second order for a long time since Abrikosov [2].

The high- T_c superconductors share a layered structure in which the superconductivity is widely believed to occur mainly in the CuO_2 layers intervened by layers of charge reservoir. This profound layer structure causes significant differences in both equilibrium and transport properties under magnetic fields in different directions. The first-order normal to superconductivity transition is mainly observed under magnetic fields perpendicular to the layers, at which the two-dimensional (2D) translation symmetry enjoyed by pancake vortices is broken. In a sharp contrast, a parallel magnetic field penetrates the system through the reservoir layers, in terms of Josephson vortices. The relevant c -axis translation symmetry is broken *a priori*, which may raise new phase and new melting process. In fact, a peculiar transport phenomenon has been found in $\text{Bi}_2\text{Sr}_2\text{CaCu}_2\text{O}_{8+y}$ by Iye et al. [3] that the resistivity does not depend on the angle between the magnetic field and current when they are both parallel to the CuO_2 layer [3] and by Ando et al. that the system shows power-law, non-Ohmic dissipations [4]. Chakravarty et al. pointed out that such a dissipation cannot occur in a lattice phase [5]. Blatter et al. [6] proposed a novel Kosterlitz-Thouless (KT) [7, 8] scenario at high magnetic fields, characterizing the behavior by a smectic state with vanishing interlayer shear modulus (see [9] for a possible KT phase at intermediate magnetic fields). Motivated by the experiment by Kwok et al. suggestive of continuous melting transition [10], Balents and Nelson proposed a smectic phase in between the lattice and liquid states and thus a two-step, continuous melting scenario at intermediate magnetic fields [11] (see [12] for a proposal of supersolid). Decoupling between superconducting layers was actually proposed even before the discovery of high- T_c superconductors [13, 14]. Starting from a 2D elastic Hamiltonian and resorting to renormalization group (RG), however, it was argued by Mikheev and Kolomeisky [15] that only a 3D long-range crystalline order is possible besides liquid state (see also [16]). The discrepancy among different approaches has not been resolved to provide a unified picture, though they provide new physical insights,

By means of computer simulations we find in the present work that there is a multicritical point in the $B - T$ phase diagram of interlayer Josephson vortices: Below the critical field, a single first-order transition upon temperature sweeping is observed; above it, there exists an intermediate KT phase characterized by in-plane 2D, quasi long-range orders (QLROs) of vortex alignment and superconductivity in between the normal phase and 3D lattice phase, accompanied by two continuous melting transitions.

The Hamiltonian is for the phases of the superconductivity order parameter on the simple cubic lattice [17, 18]

$$\mathcal{H} = -J \sum_{\langle i,j \rangle \| x,y \text{axis}} \cos(\varphi_i - \varphi_j) - \frac{J}{\gamma^2} \sum_{\langle i,j \rangle \| c \text{axis}} \cos(\varphi_i - \varphi_j - \frac{2\pi}{\phi_0} \int_i^j A_c dr_c), \quad (1)$$

where $J = \phi_0^2 d / 16\pi^3 \lambda_{ab}^2$, the y direction along the external magnetic field and $\hat{x} \perp \hat{c} \perp \hat{y}$, $\mathbf{A} = (0, 0, -xB)$, and $\gamma = \lambda_c / \lambda_{ab}$. The system is of size $L_x \times L_y \times L_c = 384d \times 200d \times 20d$ under periodic boundary conditions, with d the separation between CuO_2 layers. Vortices are identified by counting gauge invariant phase differences [17]. It was found [18] that the δ -function peak in the specific heat associated with the first-order melting of Josephson vortex lattice is suppressed when the magnetic field and/or anisotropy parameter γ exceed the critical values given

by $f\gamma = 1/2\sqrt{3}$ ($f \equiv Bd^2/\phi_0$), suggestive of a multicritical point and continuous melting(s) beyond it. In the present study, we fix $f = 1/32$ and take two typical anisotropy constants: $\gamma = 8$, realized in $\text{YBa}_2\text{Cu}_3\text{O}_{7-\delta}$ and slightly below the critical value for $f = 1/32$, and $\gamma = 20$, quite above the critical value so that analysis on the low-temperature phase becomes easier.

The first observation is made for the helicity modulus. As shown in Fig. 1, in-plane helicity moduli set up at $T \simeq 0.96J/k_B$. While the difference between the transition points of the two anisotropy parameters is very small to be seen clearly by the present system size, we differentiate them as T_m and T_{KT} for $\gamma = 8$ and $\gamma = 20$, respectively, for the reasons elucidated later. The finite helicity modulus Υ_y along the magnetic field indicates the phase coherence at low temperatures, corresponding to the breaking of U(1) gauge symmetry and therefore appearance of superconductivity. A finite value of Υ_x is a reflection of the intrinsic layer pinning (that along the c axis remains vanishing down to zero temperature). The collapse of the helicity moduli in x and y directions for $\gamma = 20$ is an intrinsic property of the state the system presumes beyond the multicritical point. It is considered to be responsible to the experimentally observed orientation independence of I-V characteristics, noting that the conductance can be evaluated by helicity moduli.

The second observation is on the density correlations of Josephson vortices. Structure factors $S[k_x, y = 0, k_c]$ at the transition points are displayed in Fig. 2. As seen in Fig. 2(a), six Bragg peaks appear for $\gamma = 8$ (see also Fig. 3), indicating that a 3D LR crystalline order is established upon the first-order freezing transition (T_m refers to the melting point). In a sharp contrast, the Bragg spots at $[\pm 2f\pi/d, \pm\pi/d]$ for $\gamma = 20$ shown in Fig. 2(b) are diffusive and stripe like. As in Fig. 3, the k_c profile of the Bragg spots for $\gamma = 20$ is fitted well by a Lorentzian function $1/[\xi_c^{-2} + (k_c - \pi/d)^2]$ with the correlation length $\xi_c \simeq 0.47d$ in the c direction. Josephson vortices are therefore decoupled into nearly independent layers at the transition point. The correlation length grows to $\xi_c \simeq 1.5d$ at $T = 0.7J/k_B$. The SR crystalline order in the c axis makes the interlayer shear modulus vanishing, which was first discussed by Blatter et al. [6].

The k_x profiles of Bragg spots at $[k_x, k_c] = [\pm 2f\pi/d, \pm\pi/d]$ for $\gamma = 20$ are plotted in Fig. 4 at several typical temperatures. Singularity appears clearly in the k_x profile below $T_{\text{KT}} = 0.96J/k_B$, consistent with the onset of the helicity moduli in Fig. 1. By fitting the profiles of the Bragg spots to the function $I \simeq a|1 - k_x d/2f\pi|^{\eta-2} + b|1 - k_x d/2f\pi| + c$, denoted in Fig. 4 by the solid curves, we estimate the exponent as $\eta \simeq 2.40 \pm 0.03, 2.21 \pm 0.01$ and $1.87 \pm 0.01, 1.41 \pm 0.02$ for $T = 0.96, 0.95$ and $0.8, 0.7J/k_B$, with the error bars from the least-squares fittings; for $T = 0.92J/k_B$ a logarithmic function fits best with the data, corresponding to $\eta = 2$; data for $T = 0.7J/k_B$ are not included for the sake of clarity. The power exponent η depends on temperature, implying that elastic constants are not simply entropy dominated as in polymer systems. The height of Bragg spots increases very slowly with decreasing temperature (see Fig. 1 of Ref.[18] for comparison). The Bragg spots become very sharp to be fitted by a power-law function for $T \leq T_\times \simeq 0.65J/k_B$; there is no difference between the shape of structure factors for $\gamma = 20$ at these low temperatures and that for $\gamma = 8$ in Fig. 2(a). These observations indicate a 3D LR crystalline order realized even in highly anisotropic systems provided temperature is low enough.

The singularities in the structure factors for $\gamma = 20$ at $T_\times < T \leq T_{\text{KT}}$ indicate unambiguously power-law density correlations, characterized by the exponent η , along the x direction in real space. Combining with the similar observations along the direction of the magnetic field, with smaller exponents, a 2D QLR crystalline order

is concluded at these intermediate temperatures. Since all 2D QLROs associated with continuous degrees of freedom known to date are governed by the KT fixed point, we identify the intermediate temperature region as a novel KT phase. The melting of this 2D Josephson vortex lattice at T_{KT} is therefore considered as a KT transition, at which the tilt modulus diminishes to zero. Since the crystalline order is SR in c direction in the KT phase, so do the gauge invariant phase correlations. The finite helicity moduli for $\gamma = 20$ below T_{KT} correspond to QLROs of phase variables.

The third observation is on the trajectories of the Josephson flux lines. This is important since a decoupling between ordered layers is argued based on RG analysis to be impossible, providing Josephson flux lines are confined completely by the CuO_2 layers [15]. As depicted in Fig. 5, hops of Josephson flux-line segments across CuO_2 layers, by creating pancake vortices, into neighboring reservoir layers are observed for $T > 0.6J/k_B$, and the percentage of hopping Josephson flux lines increases quite sharply with temperature. These observations move away the hurdle to the decoupling and the 2D phase, and thus reconcile our simulation results with the RG analysis. Hops of Josephson flux-line segments disturb intralayer correlations, weaken the interlayer correlations, as clearly seen in Fig. 4, and result in the suppression of 3D crystalline order into decoupled 2D quasi lattices for weak bare Josephson couplings. For $T \leq T_\times$, hops of Josephson flux lines are suppressed, where the argument by Mikheev and Kolomeisky should apply. As a matter of fact, this temperature regime coincides roughly with that in which the 3D LR crystalline order becomes stable for $\gamma = 20$. In Fig. 5, we also display the temperature dependence of populations of thermally excited vortex loops, and of collisions between Josephson flux lines residing in the same block layers. These results indicate clearly the importance of thermal fluctuations in the present system, and the former explains why the exponent η depends on temperature.

The evolution from the 2D QLRO to 3D LRO at T_\times is also believed to be a thermodynamic phase transition. Resorting to the effective Landau theory formulated first by Balents and Nelson [11], which works better for the present QLRO in the KT phase, it is argued that this phase transition is probably second order and in the 3D XY universality class. This observation can be taken consistent with the absence of noticeable anomaly in the specific heat at T_\times [18, 19], since the critical exponent α is slightly negative in the universality class and thus the associated cusp could be very small. The interlayer shear modulus is suppressed continuously as $C_{66} \sim (d/f\xi_c)^2$ with an exponent $2\nu \simeq 4/3$ as T_\times is approached from below.

Possible size effects on our simulation results are addressed as follows. The successful observation on the single, first-order melting transition for $\gamma = 8$ indicates that the system size is sufficient for deriving right physics below the multicritical point. Since increasing the anisotropy parameter only reduces the coupling in the c axis, the system size unlikely becomes insufficient above the multicritical point. It is easy to see that the 2D QLRO phase $[T_\times, T_{\text{KT}}]$ does not shrink to zero in the thermodynamic limit, since $T_{\text{KT}} > T_{\text{KT}}^{\text{bare}} > T_\times$, with $T_{\text{KT}}^{\text{bare}} \simeq 0.89J/k_B$, is observed under periodic boundary conditions.

Based on the analyses presented so long, we map out in Fig. 6 the $B-T$ phase diagram for interlayer Josephson vortices, noting that the same physics should occur when the magnetic field is tuned while the anisotropy parameter is fixed. The first-order melting line for low magnetic fields branches into two phase boundaries at the multicritical point $B_{mc} = \phi_0/2\sqrt{3}\gamma d^2$, containing an intermediate KT phase.

The present results are discussed in consistency with previous researches in literature: The KT phase and hops

of Josephson flux-line segments observed in the present simulations provide a clear support to the scenario by Chakravarty et al. and Blatter et al. [5, 6] formulated in order to explain the peculiar orientation independent I-V characteristics and the power-law, non-Ohmic dissipations [3, 4]. The recent experimental observation by Schilling et al. [20] on first-order melting of Josephson flux-line lattice up to 10T for $\text{YBa}_2\text{Cu}_3\text{O}_{7-\delta}$ is consistent with $B_{\text{mc}} \simeq 50T$ for $\gamma = 8$. The steep normal to superconductivity phase boundary at high magnetic fields observed by Lundqvist et al. [21] is able to be explained by the lower bound $T_{\text{KT}}^{\text{bare}}$ on $T_{\text{KT}}(B)$. Ooi and Hirata [22] detected a phase boundary on which the 3D triangular lattice softens, very similar to the one in our proposed phase diagram.

Simulations are performed on the Numerical Materials Simulator (SX-5) of NIMS. This study is partially supported by MEXT, Japan, under the Priority Grant No. 14038240.

References

- [1] G. Blatter *et al.*, Rev. Mod. Phys. **66**, 1125 (1994); G. W. Crabtree, and D. R. Nelson, Physics Today **45** 38 (1997).
- [2] A. A. Abrikosov, Zh. Eksp. Teor. Fiz. **32**, 1442 (1957) [Phys. JETP **5**, 1174 (1957)].
- [3] Y. Iye *et al.*, Physica **159C**, 433 (1989).
- [4] Y. Ando *et al.*, Phys. Rev. Lett. **67**, 2737 (1991).
- [5] S. Chakravarty *et al.*, Phys. Rev. Lett. **64**, 3187 (1990).
- [6] G. Blatter *et al.*, Phys. Rev. Lett. **66**, 2392 (1991).
- [7] V. L. Berezinsky, Sov. Phys. JETP **34**, 610 (1972).
- [8] J. M. Kosterlitz and D. J. Thouless, J. Phys. C **6**, 1181 (1973).
- [9] B. Horovitz, Phys. Rev. B **47**, 5947 (1993); *ibid* 5964 (1993).
- [10] W. K. Kwok *et al.*, Phys. Rev. Lett. **72**, 1088 (1994).
- [11] L. Balents and D. R. Nelson, Phys. Rev. Lett. **73**, 2618 (1994); *ibid* Phys. Rev. B **52**, 12951 (1995).
- [12] L. Balents and L. Radzihovsky, Phys. Rev. Lett. **76**, 3416 (1996).
- [13] K. B. Efetov, Sov. Phys. JETP **49**, 905 (1979).
- [14] B. I. Ivlev *et al.*, J. Low. Temp. Phys. **80**, 187 (1990).
- [15] L. V. Mikheev and E. B. Kolomeisky, Phys. Rev. B **43**, 10431 (1991).
- [16] S. E. Korshunov and A. I. Larkin, Phys. Rev. B **46**, 6395 (1992).
- [17] X. Hu *et al.*, Phys. Rev. Lett. **79**, 3498 (1997); P. Olsson and S. Teitel, Phys. Rev. Lett. **82**, 2183 (1999); R. E. Hetzel *et al.*, Phys. Rev. Lett. **69**, 518 (1992).

- [18] X. Hu and M. Tachiki, Phys. Rev. Lett. **85**, 2577 (2000); *ibid* **80**, 4044 (1998).
- [19] P. Olsson and P. Holme, Phys. Rev. Lett. **85**, 2651 (2000).
- [20] A. Schilling *et al.*, Phys. Rev. B **65**, 054505 (2002).
- [21] B. Lundqvist et al, Phys. Rev. B **62**, 3542 (2000); **64**, R060503 (2001).
- [22] S. Ooi and K. Hirata, Phys. Rev. Lett. **89**, 247002 (2002); private communications.

Figure captions:

Fig. 1: Temperature dependence of in-plane helicity moduli for $\gamma = 8$ and $\gamma = 20$. The universal drop of helicity modulus for a pure 2D XY model at the bare KT transition is expected at $\Upsilon \simeq 0.56J$ and $T_{\text{KT}}^{\text{bare}} \simeq 0.89J/k_B$.

Fig. 2: Structure factors at the transition point $T_{m,\text{KT}} = 0.96J/k_B$ for $\gamma = 8$ (a) and $\gamma = 20$ (b).

Fig. 3: k_c profiles of the Bragg peaks at $[k_x, k_c] = [\pm 2f\pi/d, \pm\pi/d]$ in Fig. 2. The solid curve for $\gamma = 20$ is the result of the least-squares fitting to the Lorentzian function as described in text.

Fig. 4: k_x profiles of the Bragg spots at $[k_x, k_c] = [\pm 2f\pi/d, \pm\pi/d]$ for $\gamma = 20$ at several typical temperatures. The solid curves are results of the least-squares fittings to the power-law function as described in text.

Fig. 5: Temperature dependence of ratios of Josephson flux lines which contain segments hopping into neighboring block layers, of those which hop and/or collide with neighbors in the same block layers, and populations of thermally excited, closed loops of Josephson vortices (normalized by 40×240) and those containing also pancake vortices (normalized by 240).

Fig. 6: $B - T$ phase diagram for interlayer Josephson vortices with a multicritical point. The phase boundaries $T_m(B)$, $T_{\text{KT}}(B)$ and $T_\times(B)$ are associated with first-order, KT and 3D XY phase transitions as discussed in text.

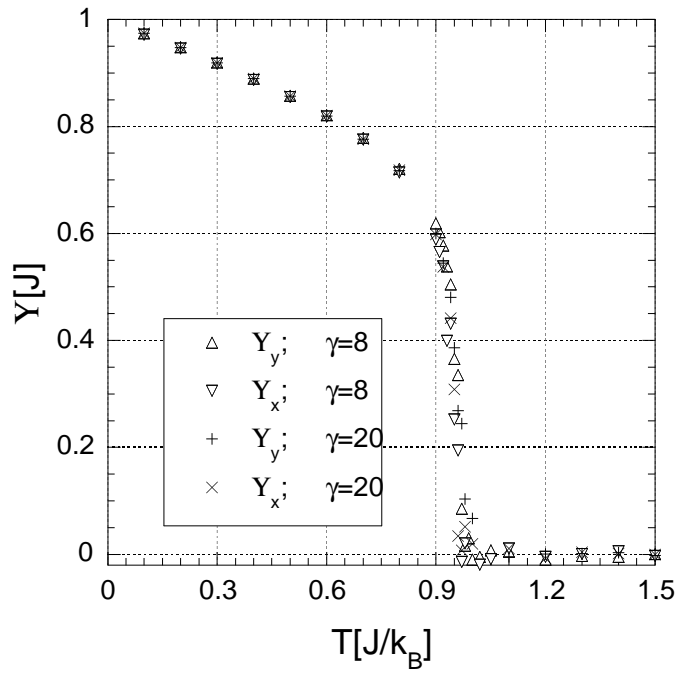


Fig. 1 by X. Hu *et al.*

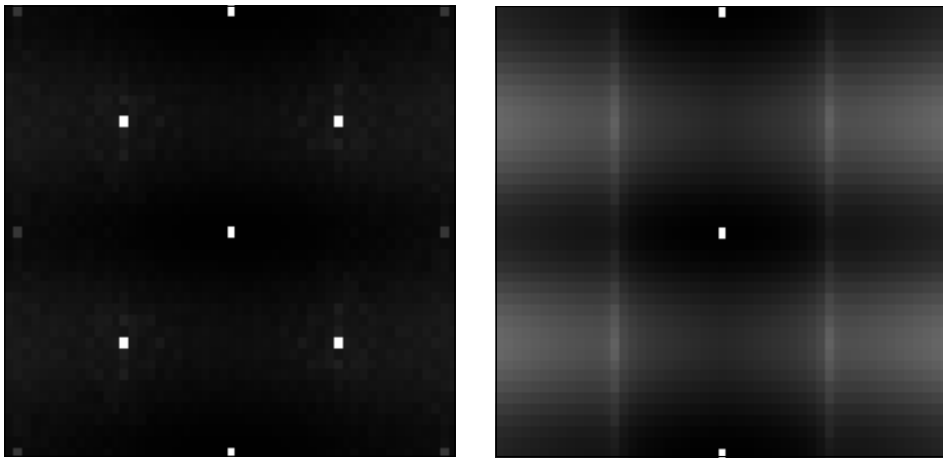


Fig. 2(a) (left) and 2(b) (right) by X. Hu *et al.*

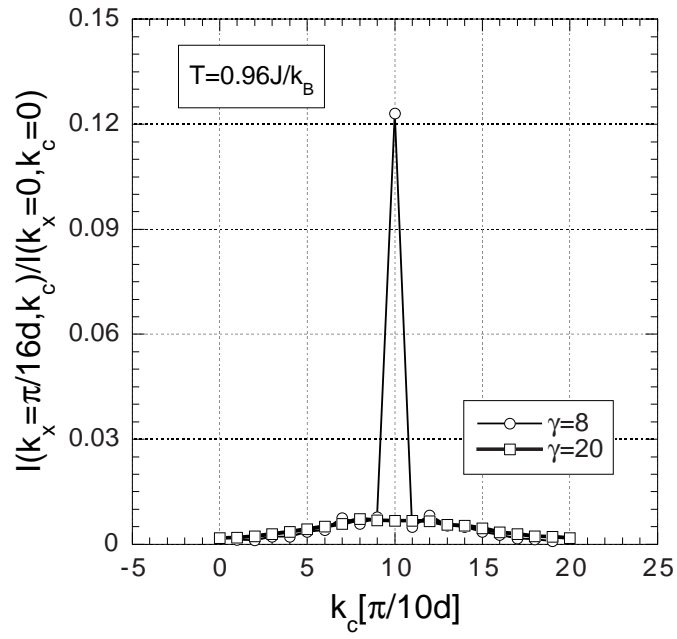


Fig. 3 by X. Hu *et al.*

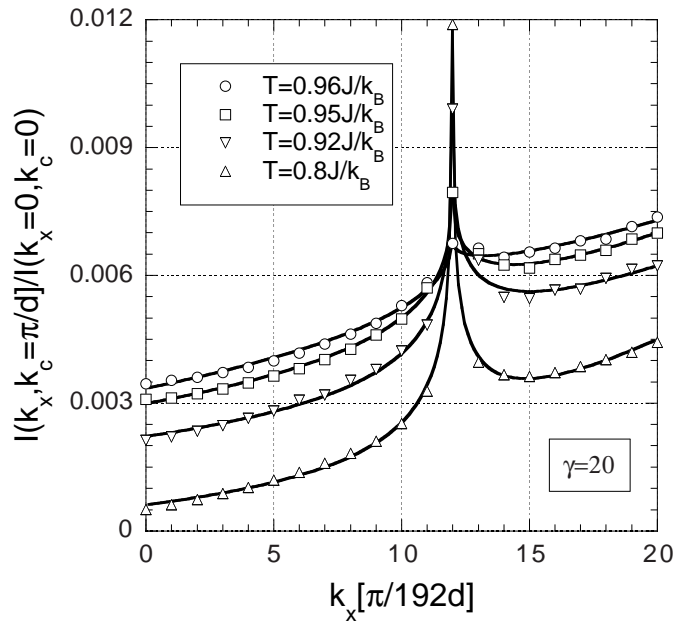


Fig. 4 by X. Hu *et al.*

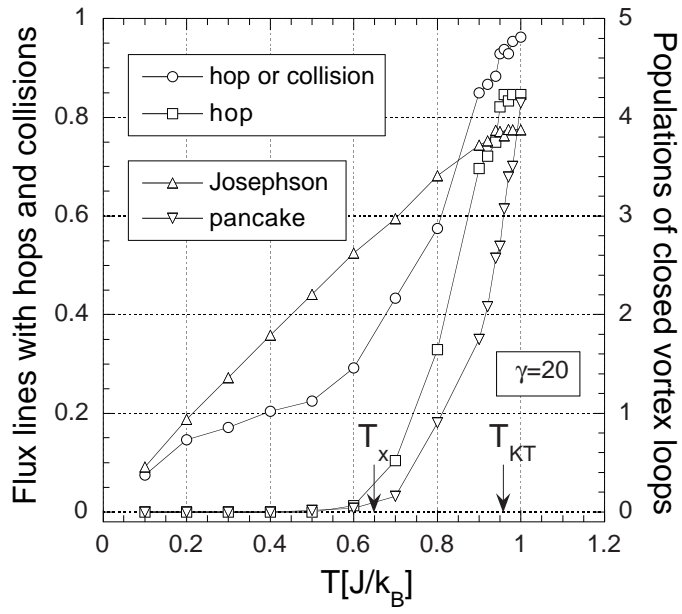


Fig. 5 by X. Hu *et al.*

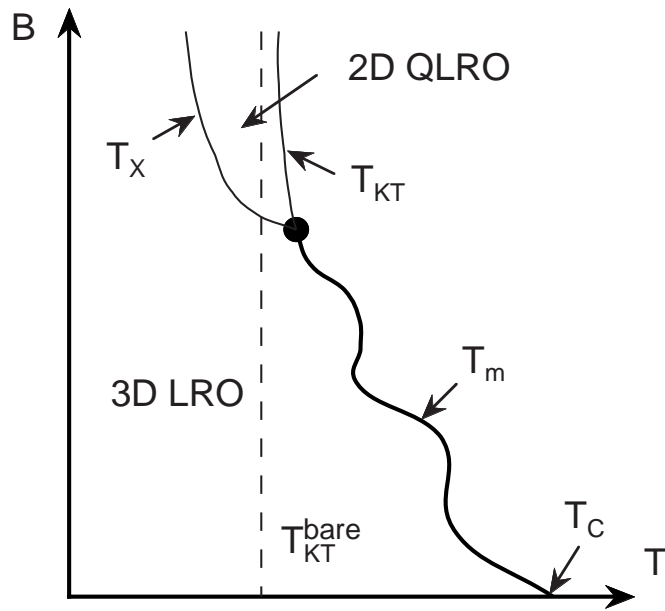


Fig. 6 by X. Hu *et al.*